12th International Symposium on Turbulence and Shear Flow Phenomena (TSFP12)
Osaka, Japan, July 19–22, 2022

PRODUCTION AND TRANSPORT OF TURBULENT HELICITY IN WALL-NORMAL ROTATING CHANNEL FLOW

Maito Horie
Institute of Industrial Science
The University of Tokyo
4-6-1 Komaba Meguro-ku, Tokyo 153-8505, JAPAN
email: maito@iis.u-tokyo.ac.jp

Fujihiro Hamba
Institute of Industrial Science
The University of Tokyo
4-6-1 Komaba Meguro-ku, Tokyo 153-8505, JAPAN
email: hamba@iis.u-tokyo.ac.jp

ABSTRACT

Turbulent helicity is known to be generated in the boundary layer when the system is rotating on an axis perpendicular to the wall. In order to investigate the production and transport mechanism, we used LES of wall-normal rotating turbulent channel flow to examine the contribution of each term in the budgets of the turbulent helicity and its three parts $\langle \bar{u}' \cdot \bar{\omega}_x{}' \rangle$, $\langle \bar{v}' \cdot \bar{\omega}_y{}' \rangle$, and $\langle \bar{w}' \cdot \bar{\omega}_z{}' \rangle$. We found that the pressure-diffusion term had the largest contribution to the generation of the turbulent helicity throughout the whole region. However, when we decompose the turbulent helicity into three terms, the contribution of the production term is the largest in the budgets of $\langle \bar{u}' \cdot \bar{\omega}_x{}' \rangle$ and $\langle \bar{w}' \cdot \bar{\omega}_z{}' \rangle$, which are superior to $\langle \bar{v}' \cdot \bar{\omega}_y{}' \rangle$. The pressure term contributes to $\langle \bar{v}' \cdot \bar{\omega}_y{}' \rangle$, and is redistributed to $\langle \bar{w}' \cdot \bar{\omega}_z{}' \rangle$ to decrease the absolute value of $\langle \bar{w}' \cdot \bar{\omega}_z{}' \rangle$. Because $\langle \bar{w}' \cdot \bar{\omega}_z{}' \rangle$ has opposite sign to $\langle \bar{u}' \cdot \bar{\omega}_x{}' \rangle$, $\langle \bar{u}' \cdot \bar{\omega}_x{}' \rangle$ becomes the biggest term of three and forms positive helicity near the wall and negative helicity away from the wall. It was shown that a subtle balance of $\langle \bar{u}' \cdot \bar{\omega}_x{}' \rangle$ and $\langle \bar{w}' \cdot \bar{\omega}_z{}' \rangle$ accounts for the profile of the total helicity.

INTROODUCTION

Fluid motions such as atmospheric and oceanic flows and convection of molten iron in the outer core are accompanied by large-scale rotational motions such as the rotation of the Earth. It has been pointed out that magnetic and fluid structures such as geomagnetic fields and typhoons are often generated and maintained by helical turbulent flow fields against eddy viscosity and anomalous resistance(Yokoi et al., 1993; Inagaki et al., 2017). The mechanisms that maintain such large-scale magnetic fields and vortices have been intensively studied especially in the field of magnetohydrodynamic flows. One of the invariants that characterize the helical motion is helicity, which is a conserved quantity defined as the inner product of velocity $\boldsymbol{u}$ and vorticity $\boldsymbol{\omega} = \boldsymbol{\nabla} \times \boldsymbol{u}$, and is known to play an important role in the α effect, one of the mechanisms of magnetic field generation in magnetohydrodynamics.

The model of helicity was proposed by Yokoi et al., (1993). In this model, the dissipation rate of helicity, $\chi_{h_{\alpha\alpha}}$, for example, can be expressed by $\chi_{h_{\alpha\alpha}} = C_h(\varepsilon/K)h$ where turbulent energy K, the dissipation rate ε, and helicity h, and C_h is model constant. However, there is no verification that discusses how accurate this model is, so we analyze the budget terms of helicity and discuss how the helicity is generated, transported, and dissipates.

In order to generate helicity, which is a pseudo-scalar quantity represented by the inner product of the axial and polar vectors, it is necessary to break a mirror symmetry. One of the methods to provide a helicity is a rotation of the system. In this study, we add a rotation of the system vertical to the wall of the channel flow. It was shown by Deusebio et al.(2014) that positive turbulent helicity is generated near the wall by production term and negative turbulent helicity is generated away from the wall by pressure diffusion term when the rotation vector of the system is vertically upward in the Ekman boundary layer.

In this study, we analyzed the production and transport mechanism of turbulent helicity by using the LES of turbulent channel flow with wall-normal rotation in order to improve the RANS turbulence model. We use LES to calculate in the case of high Reynolds numbers for future perspective. This is because to discuss the negative helicity away from the wall, we should reduce the effect from the wall for the accurate analysis. Since the turbulent helicity is distributed at low wavenumbers (Minnini, 2009), the turbulent helicity is approximated only by grid-scale physical quantities $h = \langle \boldsymbol{u}' \cdot \boldsymbol{\omega}' \rangle = \langle \bar{\boldsymbol{u}}' \cdot \bar{\boldsymbol{\omega}}' \rangle + \langle \boldsymbol{u}'' \cdot \boldsymbol{\omega}'' \rangle \sim \langle \bar{\boldsymbol{u}}' \cdot \bar{\boldsymbol{\omega}}' \rangle$ where $\langle\ \rangle$ denotes ensemble averaging, $u'(= u - \langle u \rangle)$ is the fluctuation, and $\bar{u}$ and u'' are grid-scale and subgrid-scale velocities. Here, we further decompose the helicity into three parts as $\langle \bar{u}' \cdot \bar{\omega}_x{}' \rangle$, $\langle \bar{v}' \cdot \bar{\omega}_y{}' \rangle$, and $\langle \bar{w}' \cdot \bar{\omega}_z{}' \rangle$ and examine the contribution of each term in the budget equation for each term. In this study, we deal with the case where both the rotation and Reynolds number are smaller than the study reported by Deusebio et al. (2014).

METHOD

The governing equations for the turbulent flow in a wall-normal rotating channel are grid-scale Navier-Stokes equations for an incompressible fluid. We use the SGS model

for approximating small scales. To normalize the equations, the friction velocity of the non-rotating channel flow $u_\tau = \sqrt{|\ \nu dU/dy\ |}|_{y=wall}$ is used as the velocity scale, and the half-height of the channel δ as the length scale. Then the non-dimensional equations are given as

$$\begin{aligned}\frac{\partial \bar{u}_i}{\partial t} =& -\frac{\partial}{\partial x_j}\bar{u}_i\bar{u}_j - \frac{\partial}{\partial x_i}\bar{p} \\ &+ \frac{\partial}{\partial x_j}[(\nu_S+\nu)\bar{S}_{ij}] + 2\varepsilon_{ijk}\bar{u}_j\Omega_k^F\end{aligned} \tag{1}$$

$$\frac{\partial}{\partial x_i}\bar{u}_i = 0 \tag{2}$$

where

$$\bar{S}_{ij} = \frac{\partial \bar{u}_i}{\partial x_j} + \frac{\partial \bar{u}_j}{\partial x_i} \tag{3}$$

The sketch of the wall-normal rotating channel is shown in figure 1. The boundary conditions in the x- and z-directions are periodic boundaries, and the boundary conditions in the y-direction are solid wall boundary conditions with non-slip conditions. The size of the computational domain is set to $L_x \times L_y \times L_z = 4\pi\delta \times 2\delta \times 2\pi\delta$. As shown in figure 1, the direction which has a constant pressure gradient is the x-direction, the wall vertical direction is the y-direction, and the span direction is the z-direction. The rotation axis direction is the y-direction. The channel half-width was set as δ, and the value at the center of the channel was set as the origin of the y-coordinate. Therefore, the mean pressure gradient $-\partial_x\langle p\rangle = u_\tau^2/\delta = 1$.

To solve the incompressible Grid-Scale Navier-Stokes equations (1) and (2), the second-order Adams-Bashforth method is used for the time integral, the second-order central difference is used for the spatial difference, and to solve the Poisson equation for pressure, FFT is used in the x-z directions.The number of computational grids is $64 \times 64 \times 64$, and the time width is 2.5×10^{-3}.

In the y-direction, non-uniform grid defined by equation (4) was used(Moin and Kim, 1982). For the wall function f_W attach to the eddy viscosity coefficient ν_S, the Van-Driest type equation (8) is adopted. Equation (9) is used for the model coefficients for ν_S.

$$y_j = \frac{1}{a}\tanh(b(-1+\frac{2j}{N_y}))\ \ (0 \geq j \geq N_y) = 0 \tag{4}$$

$$a = 0.98346, b = \tanh^{-1}(a) \tag{5}$$

$$\nu_S = (C_S f_W \Delta)^2\sqrt{\frac{\bar{S}_{ij}\bar{S}_{ij}}{2}} \tag{6}$$

$$\Delta = \sqrt{\Delta x \Delta y \Delta z} \tag{7}$$

$$f_W = 1 - \exp(-\frac{y_+}{A_p}) \tag{8}$$

$$C_S = 0.1, A_p = 25 \tag{9}$$

Table 1 shows the non-dimensional parameters used in this study. The Rossby number Ro_τ represents the ratio of the advection term to the Coriolis term, and the smaller it is, the more dominant the Coriolis force becomes. Since the Rossby number is quite large in this study, the Coriolis force is expected to contribute only to the mean velocity with a large spatial scale. The Ekman number Ek_τ represents the ratio of the viscous term to the Coriolis term. In this study, we discuss how helicity is generated and transported in the case of weak rotation. The equation for $\langle \bar{u_\alpha}' \cdot \bar{\omega_\alpha}' \rangle$ for grid-scale Reynolds-averaged turbulent helicity in channel flow is

$$\begin{aligned}\frac{D\langle \bar{u_\alpha}' \cdot \bar{\omega_\alpha}' \rangle}{Dt} =& P_{\alpha\alpha} + \Pi_{\alpha\alpha} + \chi_{h_{\alpha\alpha}} - \nabla \cdot t_{press_{\alpha\alpha}} \\ &- \nabla \cdot t_{turb_{\alpha\alpha}} - \nabla \cdot t_{visc_{\alpha\alpha}} + r_{\alpha\alpha}\end{aligned} \tag{10}$$

where $P_{\alpha\alpha}$: generation term, $\Pi_{\alpha\alpha}$: pressure strain correlation term, $\chi_{h_{\alpha\alpha}}$: dissipation term, $\nabla \cdot t_{press_{\alpha\alpha}}$: pressure diffusion term, $\nabla \cdot t_{turb_{\alpha\alpha}}$: turbulent diffusion term, $\nabla \cdot t_{visc_{\alpha\alpha}}$: viscous diffusion term, $r_{\alpha\alpha}$: transport term due to Coriolis force

$$P_{xx} = -\langle \bar{u}'\bar{v}' \rangle \frac{\partial \Omega_x}{\partial y} - (\langle \bar{v}'\bar{\omega}_x' \rangle - \langle \bar{u}'\bar{\omega}_y' \rangle)\frac{\partial U}{\partial y} \tag{11}$$

$$P_{zz} = -\langle \bar{v}'\bar{w}' \rangle \frac{\partial \Omega_z}{\partial y} - (\langle \bar{v}'\bar{\omega}_z' \rangle - \langle \bar{w}'\bar{\omega}_y' \rangle)\frac{\partial W}{\partial y} \tag{12}$$

$$\Pi_{\alpha\alpha} = \langle \bar{p}' \frac{\partial \bar{\omega}_\alpha'}{\partial x_\alpha} \rangle \tag{13}$$

$$\chi_{h_{\alpha\alpha}} = 2\langle [(\nu_S+\nu)\bar{S}_{\alpha j}]' \frac{\partial \bar{\omega}_\alpha'}{\partial x_j} \rangle \tag{14}$$

$$\nabla \cdot t_{press_{yy}} = \frac{\partial}{\partial y}\langle \bar{p}'\bar{\omega}_y' \rangle \tag{15}$$

$$\nabla \cdot t_{turb_{\alpha\alpha}} = \frac{\partial}{\partial y}[\langle \bar{u}_\alpha'\bar{\omega}_\alpha'\bar{v}' \rangle - \langle \bar{u}_\alpha'^2\bar{\omega}_y' \rangle] \tag{16}$$

$$\begin{aligned}\nabla \cdot t_{visc_{\alpha\alpha}} =& \frac{\partial}{\partial y}[-2\langle \{(\nu_S+\nu)\bar{S}_{\alpha y}\}'\bar{\omega}_\alpha' \rangle] \\ &+ \frac{\partial}{\partial y}[-\langle \bar{u}'\frac{\partial}{\partial x_\alpha}\{(\nu_S+\nu)\bar{S}_{z\alpha}\}' \rangle \\ &+ \langle \bar{w}'\frac{\partial}{\partial x_\alpha}\{(\nu_S+\nu)\bar{S}_{x\alpha}\}' \rangle]\end{aligned} \tag{17}$$

$$r_{yy} = 2\Omega^F \frac{\partial}{\partial y}\langle \bar{v}'^2 \rangle \tag{18}$$

Here, $\langle\ \rangle$ represents the average in the x-z plane and in time. $\alpha = x, y, z$ and no summation is taken for $\alpha\alpha$. All terms not shown in (11)-(18) are zero.

RESULT

Mean Velocity

The profiles of the mean velocity in the streamwise and spanwise directions, U and W, are shown in figures 2(a) and (b). As the rotation is imposed, the spanwise velocity W is produced and maintained. When the rotation increases, the spanwise mean velocity increases while the streamwise mean velocity decreases. Compared with Liu's DNS(Liu et.al. 2005), our LES calculations qualitatively reproduce the DNS results.

Helicity

Figure 3 shows the distribution of turbulent helicity and the intensities of turbulent helicity $\langle \bar{u}' \cdot \bar{\omega}_x' \rangle$, $\langle \bar{v}' \cdot \bar{\omega}_y' \rangle$, $\langle \bar{w}' \cdot \bar{\omega}_z' \rangle$ for $N_\tau = 0, 0.01, 0.02$. Since all of the distributions were antisymmetric across the channel, we will discuss about the lower-half of the channel. Turbulent helicity generated and maintained positive values for $-1 < y < -0.9$ and negative values for $-0.9 < y < 0$. The relationship between the sign

of the turbulent helicity and the direction of the given rotation is consistent with the results of Deusebio et al. (2014). By decomposing the turbulent helicity into three terms, we can see in which terms the turbulent helicity is dominant. $\langle \bar{u}' \cdot \bar{\omega}_x{}' \rangle$ and $\langle \bar{w}' \cdot \bar{\omega}_z{}' \rangle$ are about the same size and are 20-30 times larger than $\langle \bar{v}' \cdot \bar{\omega}_y{}' \rangle$. Since $\langle \bar{u}' \cdot \bar{\omega}_x{}' \rangle$ and $\langle \bar{w}' \cdot \bar{\omega}_z{}' \rangle$ are in opposite phases to each other, h is about 1/6 to 1/3 times as large as $\langle \bar{u}' \cdot \bar{\omega}_x{}' \rangle$, but still larger than $\langle \bar{v}' \cdot \bar{\omega}_y{}' \rangle$. Since $\langle \bar{u}' \cdot \bar{\omega}_x{}' \rangle$ is slightly larger than $\langle \bar{w}' \cdot \bar{\omega}_z{}' \rangle$, the phase of h and $\langle \bar{u}' \cdot \bar{\omega}_x{}' \rangle$ are the same. Comparing the distributions of $\langle \bar{u}' \cdot \bar{\omega}_x{}' \rangle$ and $\langle \bar{w}' \cdot \bar{\omega}_z{}' \rangle$ for each rotational parameter, both values are roughly proportional to the rotational parameter for $-1 < y < -0.9$, which is close to the wall. In contrast, for $-0.9 < y < 0$, the variation in $\langle \bar{w}' \cdot \bar{\omega}_z{}' \rangle$ is larger than that in $\langle \bar{u}' \cdot \bar{\omega}_x{}' \rangle$. In the case of $N_\tau = 0.01$, further away from the wall, at $-0.7 < y < 0$, $\langle \bar{w}' \cdot \bar{\omega}_z{}' \rangle$ had a much smaller value than $\langle \bar{u}' \cdot \bar{\omega}_x{}' \rangle$. Since the value of $\langle \bar{u}' \cdot \bar{\omega}_x{}' \rangle$ did not cancel out with the other terms, h was large enough to be compared to the peak value even near the center of the channel.

Budget of Helicity

The budgets of turbulent helicity h and its intensities in each direction are shown in figures 4 and 5. First, As it is shown in figures 3(a), 4(a) and 5(a), the positive helicity in the region around $-1 < y < -0.9$ is produced by the pressure-diffusion term, and production term with almost the same contribution. The largest contribution of the pressure-diffusion term is different from the result of Deusebio et al.(2014), where the contribution of the generation term was the largest when the rotation was stronger. On the contrary, the viscous diffusion and viscous dissipation terms contributed to attenuation of the positive helicity in this region. The viscous diffusion terms transported the positive helicity away from the wall and helped to equalize the helical structure. The viscous dissipation also generally contributed to the dissipation of the positive helicity. However, there is a gap between the point where the positive and negative helicity switched and the point where the viscous dissipation and viscous diffusion terms switched, so that around $y = -0.9$, where the helicity switched, the contribution was not in the direction of positive helicity dissipation. There isn't enough evidence to say that without looking at the spectrum of helicity, but it is thought that viscous dissipation is not simply proportional to helicity like the model of Yokoi et al., (1993) because it works on a small scale. The turbulent diffusion term works in this region to transport the positive helicity from the region a little farther from the wall to the vicinity of the wall. On the other hand, if we focus on the mechanism of negative helicity generation in the region away from the wall ($y > -0.9$), we found that the turbulent diffusion term contributes the most to the generation of negative helicity from figure 5(a) to about $-0.9 < y < -0.8$ in the same section, and the pressure diffusion term contributes the most to the generation of negative helicity at $y > -0.8$. The fact that the pressure diffusion term was effective farthest from the wall was in agreement with the study by Deusebio et al. (2014). The turbulent transport term transports the positive helicity from the lower side to the upper side of the channel and negative helicity from the upper side to the lower side of the channel. Viscous dissipation and viscous diffusion generally contribute to the reduction of the absolute value of helicity.

Next, we consider the budgets of three terms of the turbulent helicity $\langle \bar{u}' \bar{\omega}_x' \rangle$, $\langle \bar{v}' \bar{\omega}_y' \rangle$, and $\langle \bar{w}' \bar{\omega}_z' \rangle$. First, we discuss $\langle \bar{v}' \bar{\omega}_y' \rangle$, where the pressure diffusion term was the most important contributor to the generation of turbulent helicity. Figures 4 (c) and 5 (c) show that the pressure diffusion term acting on $\langle \bar{v}' \bar{\omega}_y' \rangle$ is almost balanced by the pressure strain correlation term. The pressure strain correlation term represents the redistribution from $\langle \bar{v}' \bar{\omega}_y' \rangle$ to the other terms, and since almost all of them are redistributed, $\langle \bar{v}' \bar{\omega}_y' \rangle$ itself was small and the dissipation term was also small. The redistribution was biased toward $\langle \bar{w}' \bar{\omega}_z' \rangle$ rather than $\langle \bar{u}' \bar{\omega}_x' \rangle$ (Fig. 4 and 5 (b,d)). The redistributed helicity acted to reduce the absolute value of $\langle \bar{w}' \bar{\omega}_z' \rangle$ because it was opposite to the sign of $\langle \bar{w}' \bar{\omega}_z' \rangle$. On the other hand, $\langle \bar{u}' \bar{\omega}_x' \rangle$ had no effect of redistribution and its absolute value was not reduced, so the resulting turbulent helicity h represented the same sign as $\langle \bar{u}' \bar{\omega}_x' \rangle$.

In the case of $N_\tau = 0.01$ and $N_\tau = 0.02$, where the rotation is relatively small, the pressure-diffusion term is significantly related to the turbulent helicity generation mechanism in the whole region. Near the wall, the production term was also effective. The pressure diffusion term transports the positive helicity towards the wall. Viscous dissipation and viscous diffusion generally contributed in the direction of reducing the absolute value of helicity. Looking at each of the three decomposition terms of the turbulent helicity h, $\langle \bar{u}' \bar{\omega}_x' \rangle$ and $\langle \bar{w}' \bar{\omega}_z' \rangle$, so that the magnitudes of these two terms are larger than the sum of all three terms h. Near the center of the channel, $-0.5 < y < 0$, the $\langle \bar{v}' \bar{\omega}_y' \rangle$ is generated by the pressure diffusion term and the $\langle \bar{w}' \bar{\omega}_z' \rangle$ is generated by the production term were redistributed and canceled by the pressure redistribution term. The $\langle \bar{u}' \bar{\omega}_x' \rangle$ was generated by the production term without any contribution from the other helicity by the pressure redistribution term and dissipated by the term. In addition, because of the weak rotation in this study, the transport term due to the Coriolis force had little effect on the helicity.

The variation in turbulent helicity with increasing the rotation parameter in figure 5 shows that the negative turbulent helicity decreases in the region $-0.9 < y < -0.8$. Comparing the contribution of each term in the budgets of turbulent helicity in figures 4(a) and 5(a), most of the budgets doubled when rotation parameter Ω^F doubled, however, the effect of the negative magnitude of the turbulent diffusion term decreases in this region, indicating that this change is due to the turbulent diffusion term. As for the reason for the decrease in the turbulent diffusion term, from the study of Liu et al. (2005), it is found that the turbulent energy decreases when the rotation is increased, while equation (16) shows that the turbulent energy has a positive effect on the turbulent diffusion term.

CONCLUSIONS

To discuss the generation mechanism of turbulent helicity, we evaluate the distribution of turbulent helicity and its three parts by using LES of channel turbulence rotating normal to the wall. The positive turbulent helicity is generated near the wall by the production term and pressure diffusion term and the negative turbulent helicity is generated away from the wall by the turbulent transport term and pressure diffusion term. In addition, we found that $\langle \bar{v}' \cdot \bar{\omega}_y{}' \rangle$ is generated by pressure diffusion term and is redistributed to $\langle \bar{w}' \cdot \bar{\omega}_z{}' \rangle$, which makes its absolute value smaller. Because the magnitude of $\langle \bar{u}' \cdot \bar{\omega}_x{}' \rangle$ is slightly greater than that of $\langle \bar{w}' \cdot \bar{\omega}_z{}' \rangle$, the total helicity h becomes positive near the wall, $-1 < y < -0.9$, and negative away from the wall, $-0.9 < y < 0$. It was shown that a subtle balance of $\langle \bar{u}' \cdot \bar{\omega}_x{}' \rangle$ and $\langle \bar{w}' \cdot \bar{\omega}_z{}' \rangle$ accounts for the profile of total helicity h. If we increase the parameter of the rotation to double, most of the budgets get doubled but the effect of turbulent diffusion decreases, this is because the turbulent diffusion probably monotonically decreases when turbulent energy decreases as rotation increases.

REFERENCES

[1] N. Yokoi, A. Yoshizawa, “Statistical analysis of the effects of helicity in inhomogeneous turbulence,” Physics of Fluids A: Fluid Dynamics 5,p.464, 1993.

[2] K. Inagaki, N. Yokoi, F. Hamba, “Mechanism of mean flow generation in rotating turbulence through inhomogeneous helicity,” Physical Review Fluids 2,p.114605, 2017.

[3] E. Deusebio, E. Lindborg, “Helicity in the Ekman boundary layer,” J.Fluid Mech, 755, p.654, 2014.

[4] P. Mininni, A. Pouquet, “Helicity cascades in rotating turbulence,” Physical Review E 79, p.026304, 2009

[5] P.Moin, J.Kim, ”Numerical investigation of turbulent channel flow”J.Fluid Mech,118, pp.341-377, 1982

[6] N.-D. Liu, X.-Y. Lu, “Direct numerical simulation of turbulent flows in a wall-normal rotating channel,” Journal of Turbulence, 6, No.34, 2005.

Table 1: Parameters of simulations

Re_τ	Ω^F	N_τ	Ro_τ	Ek_τ
194	0	0	∞	∞
194	0.005	0.01	200	1.03
194	0.01	0.02	100	0.515

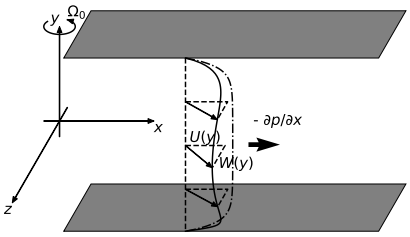

Figure 1: Configuration of wall-normal rotating channel flow

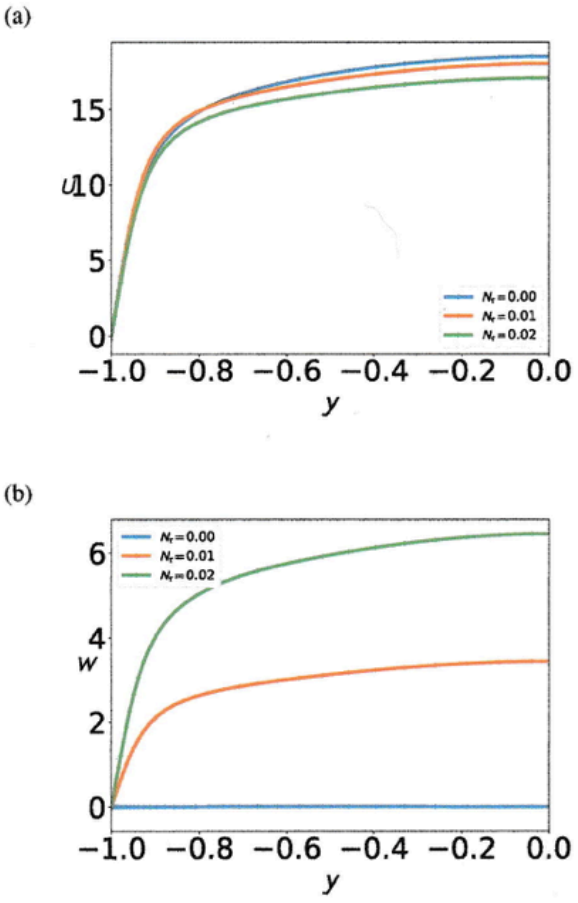

Figure 2: Profiles of the mean velocities: (a) streamwise component; (b) spanwise component

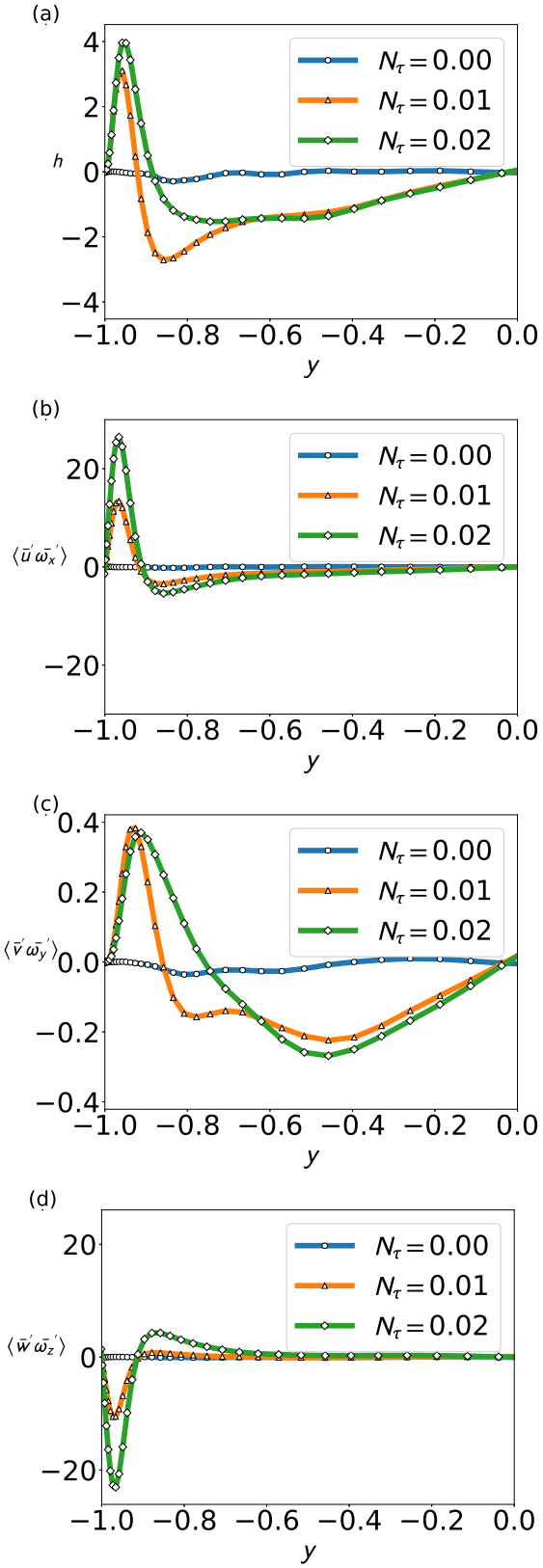

Figure 3: (a) Turbulent helicity h and its three parts, (b) $\langle \vec{u}' \cdot \bar{\omega}_x' \rangle$, (c)$\langle \vec{v}' \cdot \bar{\omega}_y' \rangle$ and (d)$\langle \vec{w}' \cdot \bar{\omega}_z' \rangle$

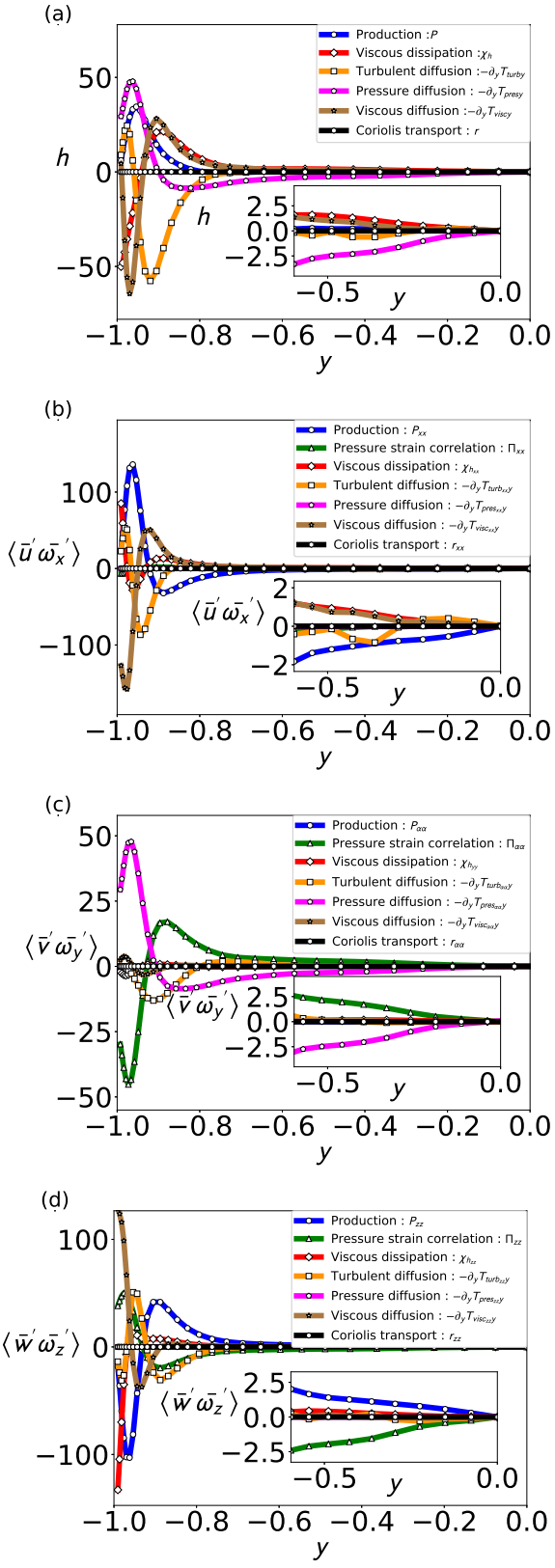

Figure 4: Budgets of (a) turbulent helicity h and its three parts (b) $\langle \bar{u}' \cdot \bar{\omega}_x' \rangle$, (c)$\langle \bar{v}' \cdot \bar{\omega}_y' \rangle$ and (d)$\langle \bar{w}' \cdot \bar{\omega}_z' \rangle$, when $N_\tau = 0.01$. The inset is the magnified view around the center of the channel.

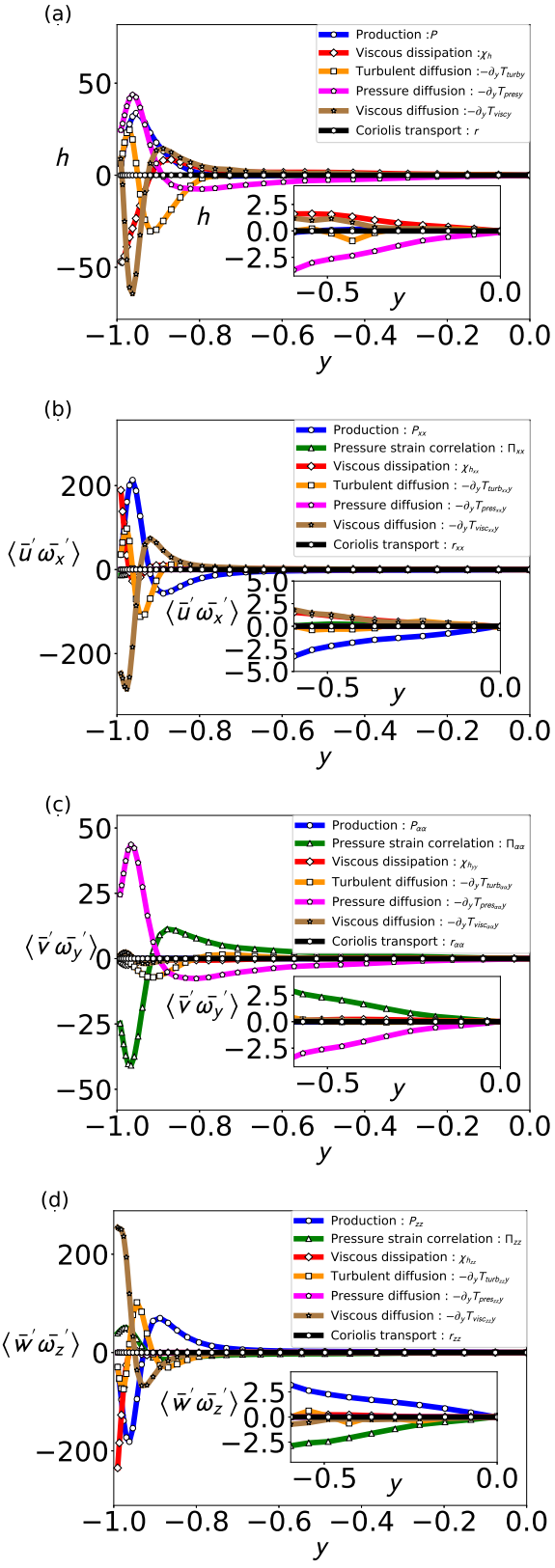

Figure 5: Budgets of (a) turbulent helicity h and its three parts (b) $\langle \bar{u}' \cdot \bar{\omega}_x' \rangle$, (c)$\langle \bar{v}' \cdot \bar{\omega}_y' \rangle$ and (d)$\langle \bar{w}' \cdot \bar{\omega}_z' \rangle$, when $N_\tau = 0.02$. The inset is the magnified view around the center of the channel.